한국소음진동공학회논문집 제 17 권 제 5 호, pp. 405~414, 2007.

A Study on Turbulent Wall Pressure Fluctuations Using a Coherent Structure Model

응집구조 모델을 이용한 난류 벽면 압력변동에 대한 연구

Byoung-Kwon Ahn†

안 병 권

(Received January 11, 2007 ; Accepted April 6, 2007)

Key Words : Turbulent Boundary Layer(난류 경계층), Wall Pressure Fluctuations(벽면 압력변동), Hairpin Vortex (헤어핀 와류), Attached Eddy Model(부착 와류모델), Eddy Number Density(와류 밀도), Wavenumber Spectrum(파수 스펙트럼), Spatial Correlation(공간 상관)

ABSTRACT

In recent years, experimental and theoretical studies show that turbulent flows looking disordered have a definite structure produced repetitively with visible order. As a core structure of turbulence, hairpin vortices are believed to play a major role in developing and sustaining the turbulence process in the near wall region of turbulent boundary layers and may be regarded as the simplest conceptual model that can account for the essential features of the wall pressure fluctuations. In this work, fully developed typical hairpin vortices are focused and the associated surface pressure distributions and their corresponding spectra are estimated. On the basis of the attached eddy model, the overall surface pressure spectra are represented in terms of the eddy size distribution. The model is validated by comparison of predicted wavenumber spectra with existing empirical models, the results of direct numerical simulation (DNS) and also spatial correlations with experimental measurements.

요 약

최근 난류유동에 대한 많은 실험 및 이론적 연구들은 무질서해 보이는 난류유동도 특정한 구조를 가지고 있으며 그 구조적 특성들이 반복적이며 가시적인 질서들을 가지고 있음을 보여주고 있다. 헤어핀 와류는 벽면 영역에서 난류경계층을 발전시키고 지탱하는 중요한 역할을 하는 난류의 핵심 구조로서 벽면 압력변동의 주요 특성을 설명해 줄 수 있는 개념 모델로 여겨지고 있다. 이 연구에서는 난류경계층에서 생성되는 헤어핀 와류들이 유기하는 표면 압력과 압력 스펙트럼을 평가하고 부착와류 모델링을 통해 이들이 유기하는 전체 표면 압력과 그에 상응하는 스펙트럼을 계산하였다. 이 연구를 통해 확립된 해석방법을 검증하기 위해 기존의 실험 및 이론계산을 통해 얻어진 결과들과 비교하여 신뢰성과 유용성을 증명하였다.

1. Introduction

The pressure fluctuations induced by turbulent boundary layers have long been of interest as a significant factor in generating vibration, and

† Corresponding Author : Member, Division of Aerospace Naval Architecture and Ocean Engineering, Chungnam National University
E-mail : bkahn@cnu.ac.kr
Tel : (042) 821-6630, Fax : (042) 823-5437

hence radiated sound, in many practical applications in which turbulent flow wets a flexible wall. The need to reduce the noise induced by boundary layers implies a requirement for a simple model capable of providing reliable insights into the characteristics of the wall pressure fluctuations.

Turbulent boundary layers exert a shear stress at the wall, and there is a strong connection between this shear stress and the structure of turbulent flows in the vicinity of the wall. Much recent empirical and numerical research has shown that the region of the flow with high vorticity near the wall appears as a bunch of hairpin vortices and longitudinal tubes. Head and Bandyopadhyay[1] investigated a turbulent boundary layer over a wide range of Reynolds number and observed hairpin vortices which are aligned at 45° to the wall and convected with a uniform velocity. While these vortices are undergoing a stretching motion, they remain straight and group together to form large scale structures, but they do not appear to be interacting strongly with each other. In flow visualization studies, many authors confirmed this feature of the hairpin vortices.

In this work, fully developed hairpin vortices inclined at an angle of 45° to the wall are focused, and their associated surface pressure distributions and corresponding spectra are estimated. On the assumption that fully developed hairpin vortices are governed by inviscid dynamics, an exact formulation for the stagnation pressure is obtained, in terms of a Green function integral along the vortex lines. The surface static pressure is then evaluated by subtracting the dynamic pressure from the results of this formulation applied to the vortex geometry.

On the basis of the attached eddy model, which implies that the form of the wave number spectrum can be deduced from the properties of a single eddy, the expressions needed for the surface pressure spectra in terms of eddy number-density are developed. This approach draws on flow visualization evidence[2], which indicates that the number of eddies observed in both stream-wise and span-wise directions of the flow is inversely proportional to their size. The overall wave number spectrum consists of contributions from eddies of all sizes, weighted by the eddy number density. The predicted wavenumber spectra are compared with those of empirical models and also with the results of DNS. The model is also validated by comparison of predicted spatial correlations with flight-test measurements.

2. Turbulent Structure and Wall Pressures

Many analytical approaches linking velocity and wall pressure fluctuations in turbulent boundary layers have been proposed. One of them, for incompressible fluctuations, begins with the Poisson equation:

$$\nabla^2 p = -\rho \frac{\partial (u_i u_j)}{\partial x_i \partial x_j} \tag{1}$$

The dominant contribution to the wall pressure fluctuations in turbulent boundary layers comes from Reynolds stresses, and the pressure field induced by turbulent flows is obtained by solving this equation. However, Reynolds stresses cannot be calculated explicitly until the complete turbulent flow is known. The traditional approach consists of determining models for Reynolds stresses based on empirical statistics so that the Navier-Stokes equation can be closed. The characteristics of the wall pressure fluctuations have been identified through spectral analysis. Significant contributions to the high wave number pressure components are attributed to activity in the near wall region, while contributions to the

low wave number components are associated with larger structures in the outer layers.

Increasingly, the importance of the coherent structures of turbulent boundary layers and their contributions to the wall pressure fluctuations is being recognized. These features help in identifying characteristics of the surface pressures and their spectra in forming a model for the pressure field beneath turbulent boundary layers. Hence a better understanding of the surface pressures induced by typical turbulent structures is required.

3. Numerical Formulation

Here the equations is derived for determining the surface pressure field induced by the hairpin vortex, which is regarded as two symmetric thin vortex lines inclined at 45° to the wall joined by a horizontal head (see Fig. 1).

In order to satisfy the wall boundary condition, image vortex lines are placed symmetrically beneath them. A suitable cut-off distance (c) and vortex core diameter (d) are adopted to avoid the singularity in the self-induction integral. The cut-off distance is thus taken as proportional to the vortex core diameter which is also proportional to the distance between the two legs.

Starting from the Navier-Stokes equation for an incompressible flow and using the vector identity, $(\overline{u}\cdot\nabla)\overline{u}=\nabla(\frac{1}{2}\overline{u}\cdot\overline{u})-\overline{u}\times\overline{\omega}$, and introducing the stagnation pressure, $p(x,t)=p'+\frac{1}{2}\rho|\overline{u}|^2$, the momentum equation may be written in the form

$$\rho\left(\frac{\partial\overline{u}}{\partial t}+\overline{\omega}\times\overline{u}\right)=-\nabla p+\mu\nabla^2\overline{u} \tag{2}$$

Taking the divergence of each term in Eq. (2) and using the continuity equation for an incompressible flow, the Poisson equation for the stagnation pressure can be obtained:

$$\nabla^2 p=-\rho\nabla\cdot(\overline{\omega}\times\overline{u}) \tag{3}$$

The solution of the Poisson equation can be determined in terms of the Green function $G(Y|X)$:

$$G(Y|X)=\frac{-1}{4\pi|Y-X|}+\frac{-1}{4\pi|Y-X^*|} \tag{4}$$

where $Y=(y_1,y_2,y_3)$ is the field point, and $X^*=(x_1,x_2,-x_3)$ is the image point of $X=(x_1,x_2,x_3)$.

The stagnation pressure is written in terms of a volume integral over the region in which the vorticity is not zero, and a surface integral due to viscous effects,

$$p(X,t)=\int_V \nabla G\cdot\rho(\overline{\omega}\times\overline{u})\,d^3y + \int_S \mu G\nabla^2 u_3\,dy_1dy_2 \tag{5}$$

Figure 2 shows the static pressure fields on the surface for different aspect ratios. It concludes that when L is larger than 10λ the effect of the head is almost insignificant. As the aspect ratio decreases from this value, however, the pressure field shows marked quantitative and qualitative differences, eventually changing from being essentially positive in $x>0$, and negative in $x<0$, to the opposite by $L/\lambda=0.5$.

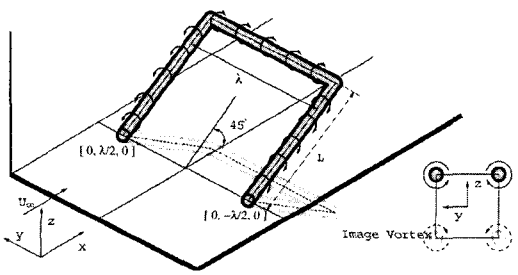

Fig. 1 Configuration for the hairpin vortex model

4. Spectral Quantities

In experimental works, Perry et al[2] showed

that an isolated hairpin vortex undergoes a stretching motion in which the vortex height L increases uniformly with time and the distance λ between the two legs of the hairpin vortex at the wall decreases such that the product λL remains constant. They also showed a geometrically similar random array of hairpin vortices exists in the turbulent wall region and all eddy arrays have the same velocity scale ($\sim u_\tau$). They applied the observation that the only velocity scale in the log-law region is the friction velocity (u_τ) to each individual eddy. Thus the typical hairpin vortex, with length scale λ, has vorticity $\omega \sim u_\tau \lambda^{-1}$ and circulation $\Gamma \sim u_\tau \lambda$.

Flow visualization work that they cite indicates that the number of eddies observed in both stream-wise (x) and span-wise (y) directions decreases like λ^{-1}. This implies that the number of eddies per unit area around a scale λ should be four times that around the scale 2λ, and this requirement is fulfilled by the eddy number density $n(\lambda) = N\lambda^{-3}$, with N constant. The physical interpretation of the increase in circulation with size is linked to the λ^{-1} distribution of eddies in the stream-wise direction, which implies

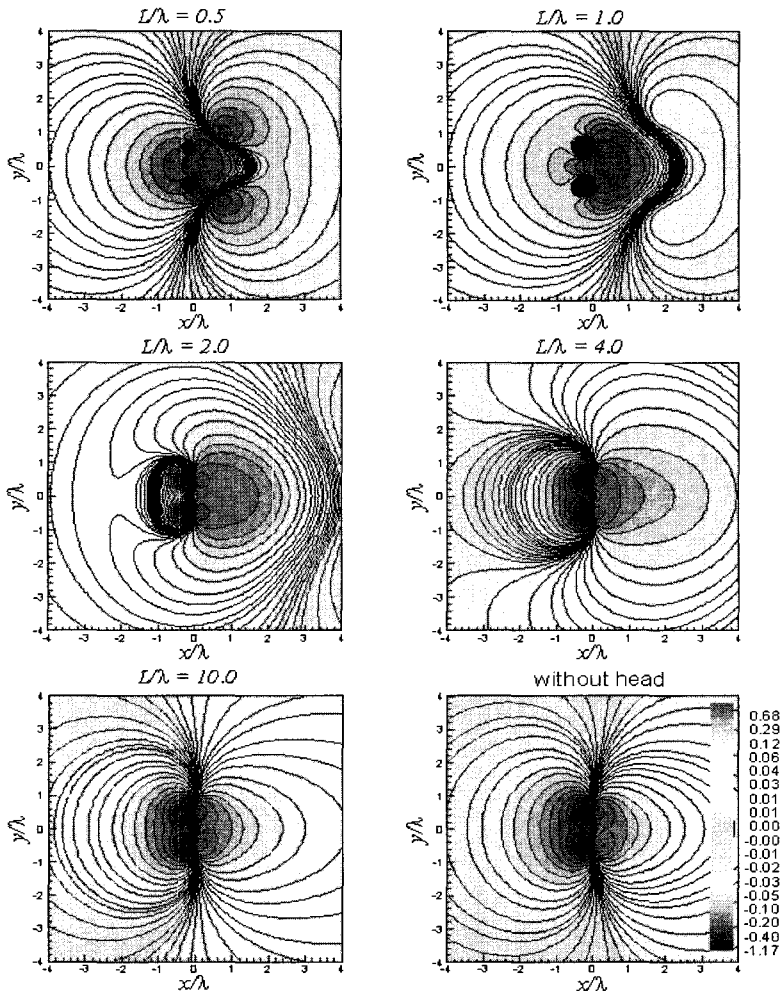

Fig. 2 Surface pressure contours according to different eddy aspect ratios

combination as they evolve and grow.

The key point in deriving spectra from the attached eddy model is that the eddies are not correlated (on average). This implies that the form of a spectrum can be deduced from the properties of a single eddy. This approach is applied to velocity auto and cross-spectra by Perry et al[2], but it can be equally well used for pressure spectra. Here, an alternative approach is developed, in terms of eddy number density, to obtain expressions needed for the surface pressure spectra. The wavenumber spectrum is defined by

$$S(k_x,k_y)=dint_{-\infty}^{\infty}R(\xi,\eta)e^{-i\xi k_x}e^{-i\eta k_y}d\xi d\eta \quad (6)$$

with $R(\xi,\eta)$ the spatial correlation of the surface pressure, where ξ and η are space separations.

$$R(\xi,\eta)=\overline{p(x,y)p(x+\xi,y+\eta)} \quad (7)$$

It can be related to the Fourier transform of the pressure field,

$$P(k_x,k_y)=dint_{-\infty}^{\infty}p(x,y)e^{-i\xi k_x}e^{-i\eta k_y}dxdy \quad (8)$$

via generalized function theory[3], with the result that

$$(2\pi)^2\delta(k_x+k_x')\delta(k_y+k_y')S(k_x,k_y) = \overline{P(k_x,k_y)P(k_x',k_y')} \quad (9)$$

The pressure field arising from all eddies is

$$P(k_x,k_y)=\sum_{N_e}P_e(x-x_e,y-y_e,\lambda) \quad (10)$$

where (x_e,y_e) is the eddy location. The Fourier transform is thus

$$P(k_x,k_y)=\sum_{N_e}P_e(k_x,k_y,\lambda)e^{-ik_x x_e}e^{-ik_y y_e} \quad (11)$$

where N_e is the eddy number density and $P_e(k_x,k_y,\lambda)$ is the Fourier transform of the pressure field due to an individual eddy. Note that the ensemble average has removed all terms involving contributions from different eddies. Then the summation is replaced with an integral over eddy location and scale, giving

$$(2\pi)^2\delta(k_x+k_x')\delta(k_y+k_y')S(k_x,k_y) = \int_{\lambda_m}^{\delta}dint_{-\infty}^{\infty}n(\lambda)P_e(k_x,k_y,\lambda)P_e(k_x',k_y',\lambda) e^{-i(k_x+k_x')x_e}e^{-i(k_y+k_y')y_e}dx_e dy_e d\lambda \quad (12)$$

Here λ_m is the scale of the smallest eddy (around $100\nu/u_\tau$), and δ the boundary layer thickness which is the scale of the largest eddy. Integration over k_x' and k_y' now yields

$$S(k_x,k_y)=\int_{\lambda_m}^{\delta}n(\lambda)|P_e(k_x,k_y,\lambda)|^2d\lambda \quad (13)$$

In the same way, the stream-wise and span-wise spectrum are respectively expressed as follow:

$$S(k_x,\eta=0)=\int_{\lambda_m}^{\delta}\int_{\infty}^{\infty}n(\lambda)|P_e(k_x,y,\lambda)|^2dyd\lambda \quad (14)$$

$$S(\xi=0,k_y)=\int_{\lambda_m}^{\delta}\int_{\infty}^{\infty}n(\lambda)|P_e(x,k_y,\lambda)|^2dxd\lambda \quad (15)$$

Figure 3 shows parameter studies presenting the influence of varying $\hat{\lambda}_{max}(\lambda_{max}/\delta)$ and $\hat{\lambda}_{min}(\lambda_{min}/\delta)$ values for the eddy aspect ratio, $L/\lambda=10.0$. A -1 slope clearly appears in both stream-wise and span-wise spectra. As the largest eddy scale ($\hat{\lambda}_{max}$) decrease, the spectrum's level decreases and its peak or roll-off appears at higher wavenumber regions. When the smallest eddy scale ($\hat{\lambda}_{min}$) increases the spectrum's level collapses earlier.

5. Model Validation

5.1 Comparison with Empirical Models

The purely empirical models discussed in earlier work by Graham[4] were those of Corcos[5], Efimtsov[6], and Smol'yakov and Tkachenko[7]. Of these, the Corcos model is compromised by having no dependence of correlation length on boundary layer thickness, so it is restrict to the latter two in this work. Efimtsov follows Corcos in postulating a model of the form

$$R(\xi, \eta, \omega) = \Phi(\omega) e^{-|\xi|/\Lambda_x} e^{-|\eta|/\Lambda_y} e^{i\omega\xi/U_c} \quad (16)$$

In Eq. (16), $\Phi(\omega)$ is the point pressure spectrum, $R(0,0,\omega)$, U_c is a (frequency-dependent) convection velocity and Λ_x, Λ_y are correlation length scales. Corresponding one-dimensional wavenumber frequency spectra are

$$S(k_x, \eta = 0, \omega) = \frac{2\Phi(\omega)\Lambda_x}{[1 + \Lambda_x^2 (k_x - \omega/U_c)^2]} \quad (17a)$$

$$S(\xi = 0, k_y, \omega) = \frac{2\Phi(\omega)\Lambda_y}{[1 + (k_y \Lambda_y)^2]} \quad (17b)$$

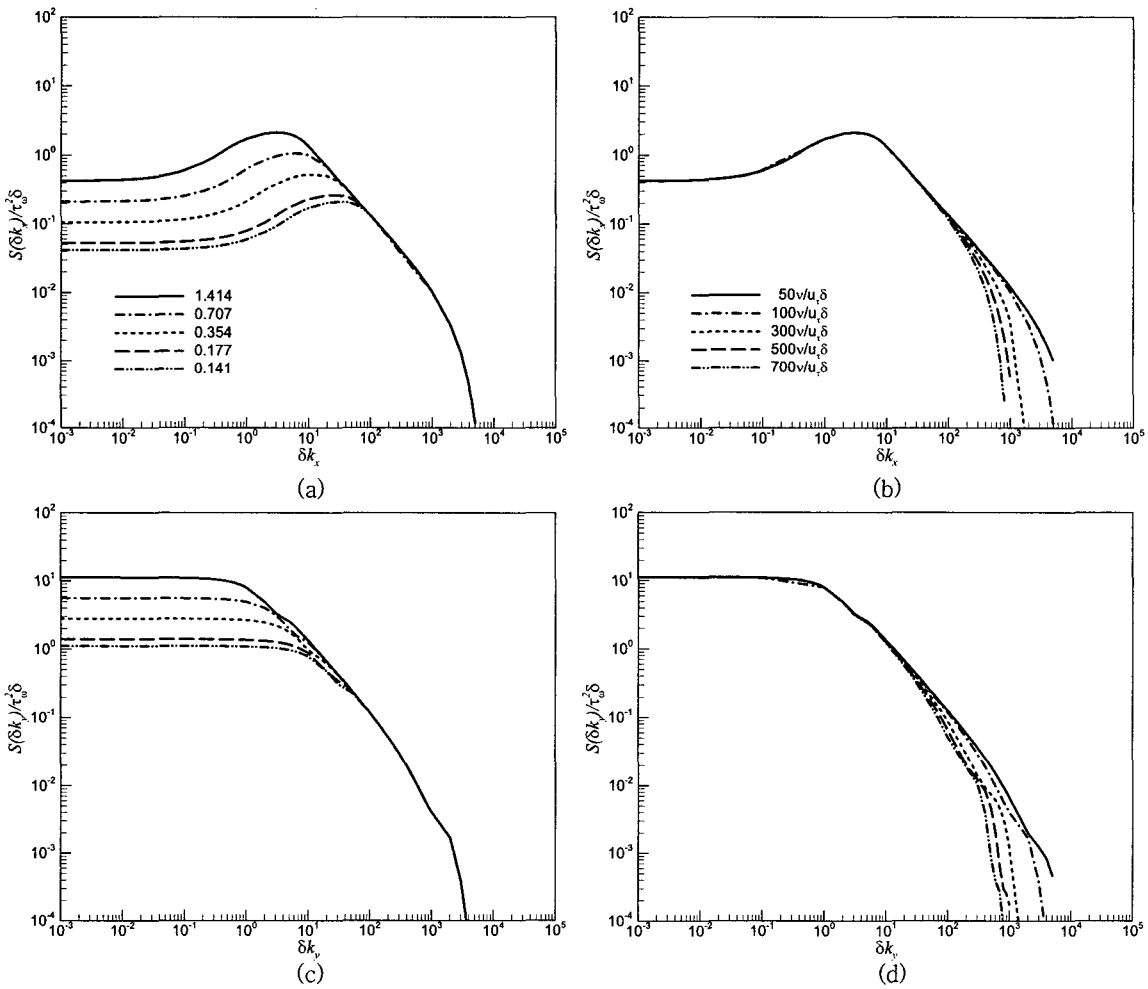

Fig. 3 Parameter study for the eddy aspect ratio $L/\lambda = 10.0$. Stream-wise wavenumber spectra : (a) varying the largest eddy scales from 1.414 to 0.141; (b) varying the smallest eddy scales from 50 to $700v/u_\tau\delta$; Span-wise wavenumber spectra; (c) varying the largest eddy scales from 1.414 to 0.141; (d) varying the smallest eddy scales from 50 to $700v/u_\tau\delta$

The one-dimensional wavenumber frequency spectra of Eq. (17a) and (17b) are unaffected by this choice, but the two-dimensional spectrum becomes

$$S(k_x, k_y, \omega) = \frac{\Phi(\omega)\Lambda_x\Lambda_y}{[1+\Lambda_x^2(k_x-\omega/U_c)^2+(k_y\Lambda_y)^2)]^{3/2}} \quad (18)$$

Many authors have proposed curve fits for this quantity; for consistency, an initial choice for the model is that proposed by Efimtsov;

$$\Phi_E(\omega) = \frac{\tau_\omega^2\delta}{u_\tau}\frac{0.01\pi}{[1+0.02(\omega\delta/u_\tau)^{2/3}]} \quad (19)$$

This form, however, has a major drawback, in that its integral is undefined. However, a form that addresses these issues is also desirable, and here the modified expression is used.

$$\Phi_B(\omega) = \frac{\tau_\omega^2\delta^*}{U_\infty}\frac{2\pi 8.28(\omega\delta^*/u_\tau)^{0.8}}{K}$$
$$K = [1+4.1(\omega\delta^*/u_\tau)^{1.7}+4.4\times10^{-4}(\omega\delta^*/u_\tau)^{5.9}] \quad (20)$$

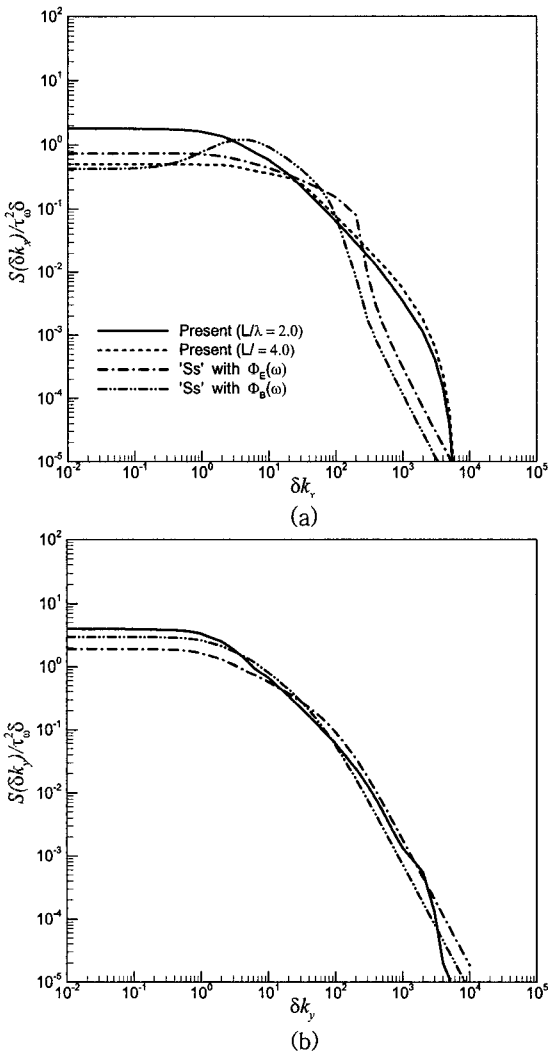

Fig. 4 Comparison of predicted wavenumber spectra with empirical models. (a) stream-wise; (b) span-wise

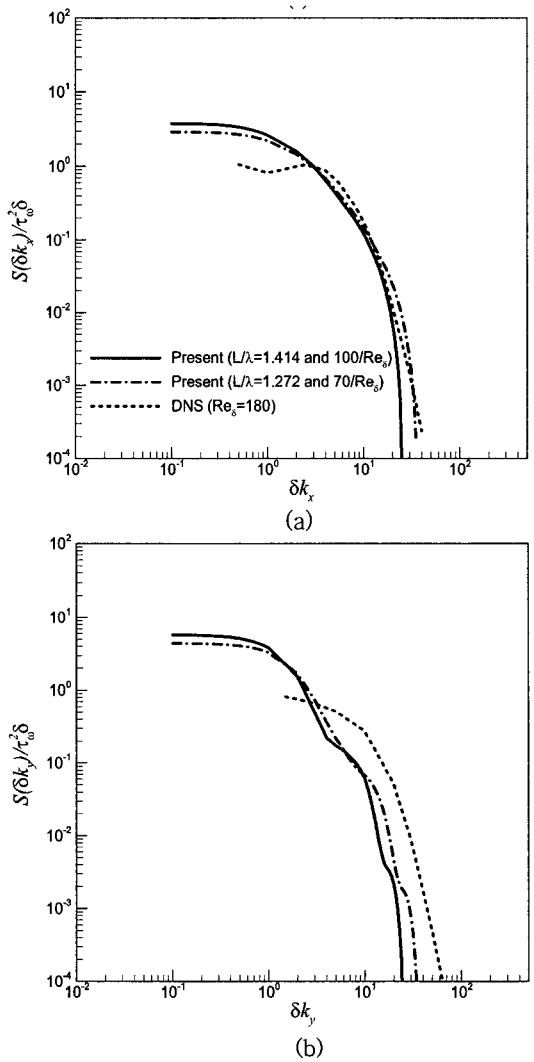

Fig. 5 Comparison of predicted wavenumber spectra with DNS results. (a) stream-wise; (b) span-wise

where δ^* is the boundary layer displacement thickness. Eq. (20) is Ahn's estimate[8] of the best curve-fit to Blake's[9] smooth wall data.

The associated one-dimensional spectra are shown over a wide range (and hence on logarithmic scales) in Fig. 4. Here it is first clear that the agreement is best for the lateral spectrum, with the two best-fit pairs matching closely in both initial level and rate of roll-off. An extended k^{-1} region is clearly visible. In contrast, the longitudinal spectra derived from empirical models show either no such region (using $\Phi_E(\omega)$) or a very limited one (using $\Phi_B(\omega)$). The attached eddy model spectra again have an extensive k^{-1} region, and hence roll off less quickly than their empirical counterparts.

5.2 Comparison with DNS Results

The difficulty in making comparisons with DNS can be illustrated by closer consideration of the limits for the scale integrals of Eqs. (13), (14) and (15). Recall that, on physical grounds, it is expected $\hat{\lambda}_{min}=100/R_{e_\delta}$ and $\hat{\lambda}_{max}=\sqrt{2}\lambda/L$, where $R_{e_\delta}=u_\tau\delta/\nu$. For $R_{e_\delta}\sim100$, typical of the DNS, there is thus no range of eddy scales to integrate over if $L/\lambda>\sqrt{2}$. Physically, then, the concept of a hierarchy of eddies, central to the attached eddy model, is dubious at these Reynolds numbers. With this caveat, the agreement between the model is investigated, using low values of L/λ, and the DNS data of Choi and Moin[10], for which $R_{e_\delta}(u_\tau\delta/\nu)=180$.

For eddies with $L/\lambda=1$, it has $\hat{\lambda}=0.556$ and $\hat{\lambda}=1.414$; any significant increase in L/λ would make this range unfeasibly small, so higher aspect ratio eddies are not considered. The overall levels of the predicted spectra are set by the requirement that they should integrate to give the same mean square pressure as the DNS, which, because of the low Reynolds number, is only $(1.5\tau_\omega)^2$. The results are compared with the DNS data in Fig. 5, where it shows generally good agreement for the longitudinal spectra, except at low wavenumber regions, but a slightly early roll-off in the lateral prediction. A small change in the parameters $\hat{\lambda}$ and $\hat{\lambda}$, to 0.389 and 1.272 respectively, reduces this discrepancy to some extent, but it has no physical justification for this choice. Note also the oscillations in the predicted lateral spectra, remnants of the lobed structure seen in the corresponding universal spectrum, which has not been fully averaged out in this limited scale integral.

5.3 Comparison with Experimental Data

Here the predictions of the model with data measured by NASA Langley Research Center are compared. NASA measured fuselage surface pressures, panel vibrations and interior noise levels on a Tu-144LL aircraft (see Rizzi et al[11] for details). The corresponding boundary layer parameters required for the model are set out in Table 1. Note that no measurements of boundary layer thickness are available; the values given here are calculated from empirical American (δ_u) and Russian (δ_r) expressions cited by Rizzi et al.[11]

Figure 6 shows the resulting model predictions, for $L/\lambda=1$ and 2 (with $\hat{\lambda}_{max}$ set accordingly), and the experimental data. The normalized correlation function is plotted against ξ/δ and η/δ so the same absolute experimental separation

Table 1 Boundary layer parameters used in the model

Mach number (M)	0.74
Altitude	5.0 km
Free stream speed of sound (a)	320.545 m/s
Kinematic viscosity (ν)	$2.2\times10^{-5}m^2/s$
Reynolds number (lU/ν)	5.574×10^8

where l is the distance from aircraft nose, and $U=M\times a$.

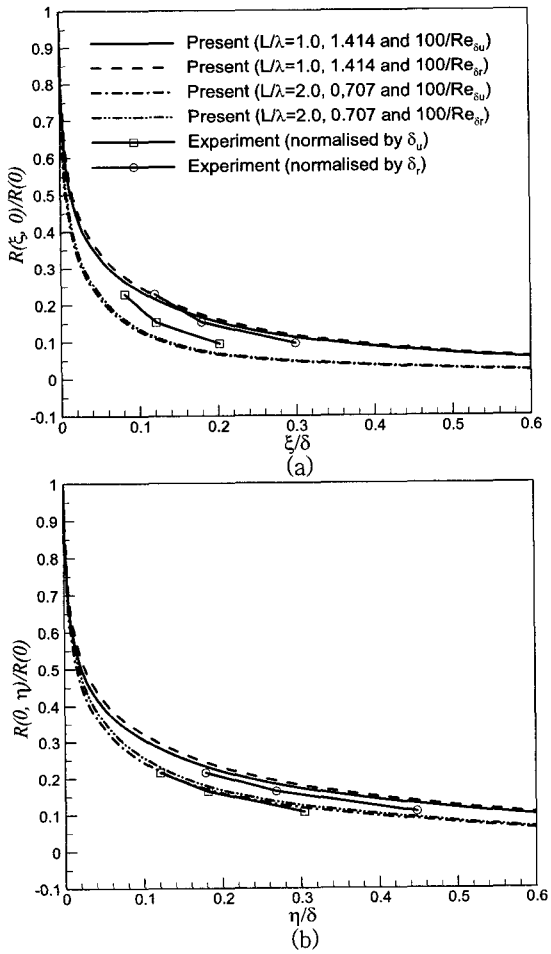

Fig. 6 Comparison of spatial correlations. (a) stream-wise; (b) span-wise

gives rise to two experimental points, corresponding to the American and Russian boundary layer thicknesses. Similarly, $\hat{\lambda}$ varies according to the choice of δ, but this has an almost negligible effect on the predictions. Changing the aspect ratio is much more influential; increasing L/λ from 1 to 2 noticeably decreases both longitudinal and lateral correlation lengths. These aspect ratios span the variation in experimental data due to the different estimates of δ; the use of δ_r gives results closely predicted by the $L/\lambda = 1$ curve, while δ_u leads to values in agreement with $L/\lambda = 2$.

6. Conclusions

In this paper it is applied the formulation for the pressure field associated with a given vorticity distribution in an incompressible fluid to calculate the wall pressures associated with a typical hairpin vortex. The attached eddy hypothesis is then used to derive the instantaneous wavenumber spectra of the pressures due to an ensemble of such eddies of varying size. The form of these spectra depends on three model parameters; the minimum and maximum eddy size, and the aspect ratio, L/λ, of the ensemble members. Specifically, reducing the minimum size increases spectral levels at high wavenumber, while increasing the maximum size does the same at low wavenumber. Increasing the aspect ratio introduces a peak in the intermediate wavenumber region of the longitudinal spectrum, but has minimal effect on the shape of the lateral spectrum.

The model was tested by comparison with: (i) high Reynolds number instantaneous spectra derived from empirical expressions for wavenumber frequency spectra; (ii) low Reynolds number instantaneous spectra from DNS results; (iii) high Reynolds number spatial correlations measured in flight tests. In all cases, the level of agreement is encouragingly good, given the simplicity of the model.

The paper concludes that this coherent structure model shows considerable promise in describing wall pressures underneath high Reynolds number turbulent boundary layers, and is therefore potentially useful for investigating details of their structure that are currently inaccessible via other techniques. However, more detailed validation against high spatial resolution experimental data is probably required before it can be employed with complete confidence.

Acknowledgement

The author would like to thank Dr. Will Graham of the University of Cambridge, and Dr. Stephen Rizzi of NASA Langle Research Center for their helpful discussions.

References

(1) Head, M. R. and Bandyopadhyay, P., 1981, "New Aspect of Turbulent Structure", Journal of Fluid Mech., 107, pp. 297~338.

(2) Perry, A. E., Henbest, S. and Chong, M. S., 1986, "A Theoretical and Experimental Study of Wall Turbulence", Journal of Fluid Mech., 165, pp. 163~199.

(3) Dowling, A. P. and Ffowcs Williams, J. E., 1989, Sound and Sources of Sound, Ellis Horwood Limited, Chapter 10.

(4) Graham, W. R., 1997, "A Comparison of Models for the Wavenumber-frequency Spectrum of Turbulent Boundary Layer Pressures", Journal of Sound and Vibration, Vol. 206, No. 4, pp. 541~565.

(5) Corcos, G. M., 1964, "The Structure of the Turbulent Pressure Field in Boundary-layer Flows", Journal of Fluid Mech., Vol. 18, No. 3, pp. 353~378.

(6) Efimtsov, B. M., 1982, "Characteristics of the Field of Turbulent Wall Pressure Fluctuations at Large Reynolds Numbers", Sov. Phys. Acoust., Vol. 28, No. 4, pp. 289~292.

(7) Smol'yakov, A. V. and Tkachenko, V. M., 1991, "Model of a Field of Pseudosonic Turbulent Wall Pressures and Experimental Data", Sov. Phys. Acoust. Vol. 37, No. 6, pp. 627~631.

(8) Ahn, B., 2005, Modelling Unsteady Wall Pressures Beneath Turbulent Boundary Layers, Ph. D. thesis, University of Cambridge.

(9) Blake, W. K., 1970, "Turbulent Boundary-layer Wall-pressure Fluctuations on Smooth and Rough Walls", Journal of Fluid Mech., 44, pp. 637~660.

(10) Choi, H. and Moin, P., 1990, "On the Space-time Characteristics of Wall-pressure Fluctuations", Physics of Fluids, 2, pp. 1450~1460.

(11) Rizzi, S. A., Rackl, R. G. and Andrianov, E. V., 2000, Flight Test Measurements from the Tu-144L Structure/Cabin Noise Experiment, NASA Tech. Mem. 2000-209858.